Electron Spin Resonance

Parth Bhargava (A0310667E)

Experiment A · September 12, 2025

1 Abstract

This experiment investigated electron spin resonance (ESR) in diphenyl-picryl-hydrazyl (DPPH), a stable free radical, to determine the g-factor of its unpaired electron. ESR absorption was observed by subjecting the DPPH sample to a static magnetic field generated by Helmholtz coils and a radio frequency (RF) alternating magnetic field. Resonance frequencies ranging from 30 to 76.6 MHz were applied while measuring the corresponding magnetic fields at resonance conditions. Linear regression analysis of the frequency-field relationship yielded a g-factor of $g_s = 1.905 \pm 0.025$, deviating by 4.9% from the theoretical value of 2.0036. The experiment demonstrates the fundamental quantum mechanical phenomenon of electron spin splitting in magnetic fields and validates the ESR technique for characterizing paramagnetic materials.

2 Background and Objectives

Electron spin resonance (ESR), also known as electron paramagnetic resonance (EPR), is a spectroscopic technique used to study materials with unpaired electrons. The phenomenon arises from the interaction between the magnetic moment of unpaired electrons and an external magnetic field, making it invaluable for investigating free radicals, transition metal complexes, and defects in solids.

The theoretical foundation of ESR lies in the quantum mechanical behavior of electron spin. An electron possesses an intrinsic angular momentum characterized by spin quantum number $S = \frac{1}{2}$, with only two possible projections along any axis: $S_z = \pm\frac{\hbar}{2}$. The associated magnetic moment is given by:

$$\boldsymbol{\mu_s} = -\frac{g_s \mu_B}{\hbar}\boldsymbol{S} \tag{1}$$

where g_s is the g-factor (approximately 2.0036 for a free electron), $\mu_B = 9.274 \times 10^{-24}$ J/T is the Bohr magneton, and $\hbar$ is the reduced Planck constant.

In an external magnetic field B, the energy levels split according to:

$$E = E_0 \pm \frac{1}{2} g_s \mu_B B \tag{2}$$

This Zeeman splitting creates two energy levels separated by $\Delta E = g_s \mu_B B$. Resonance absorption occurs when electromagnetic radiation of frequency f satisfies the resonance condition:

$$hf = \Delta E = g_s \mu_B B \tag{3}$$

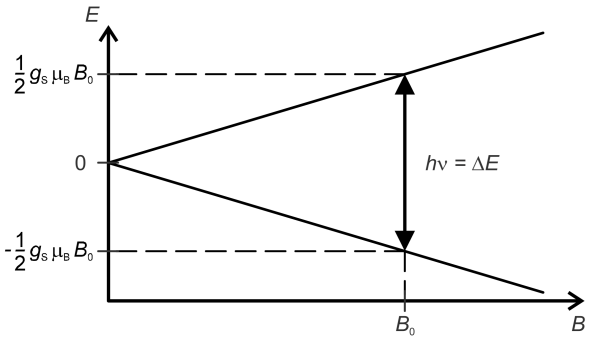

Figure 1: Splitting of energy levels in an external B-field

The objective of this experiment was to determine the g-factor of DPPH by measuring the relationship between resonance frequency and magnetic field strength, thereby validating the fundamental principles of ESR spectroscopy.

3 Experimental Methods

3.1 Apparatus and Sample

The experimental setup consisted of a pair of Helmholtz coils (320 turns each, radius $R = 6.8$ cm) for generating the static magnetic field, a radio frequency oscillator (15-300 MHz range), an ESR control unit with integrated ammeter, and a cathode ray oscilloscope for signal detection. The sample was diphenyl-picryl-hydrazyl (DPPH), an organic free radical with chemical formula $C_{18}H_{12}N_5O_6$, chosen for its stability and well-characterized ESR properties.

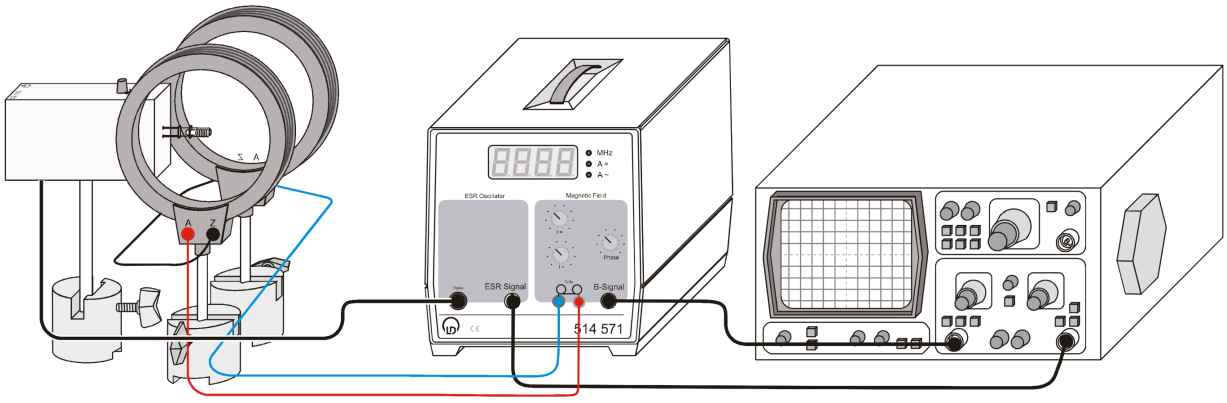

Figure 2: Schematic of the experimental setup.

The Helmholtz coils were connected in series to ensure uniform field generation. The magnetic field at the center of the coil pair is given by:

$$B = \mu_0 \left(\frac{4}{5}\right)^{\frac{3}{2}} \frac{nI}{R} \tag{4}$$

where $\mu_0 = 4\pi \times 10^{-7}$ T · m/A is the permeability of free space, $n = 320$ is the number of turns per coil, I is the current, and R is the coil radius.

3.2 Experimental Procedure

The DPPH sample was placed at the center of the Helmholtz coils within a high-frequency coil connected to the RF oscillator. A 50 Hz modulation was superimposed on the DC magnetic field

to enable phase-sensitive detection. The oscilloscope was configured in X-Y mode with the following settings: Y-channel at AC 0.2-1 V/cm for the ESR signal, X-channel at AC 2 V/cm for the modulation signal, and time base at 1 ms/cm.

For each measurement, the RF frequency was set to a specific value between 30-80 MHz. The DC current through the Helmholtz coils was then carefully adjusted while monitoring the oscilloscope display. The resonance condition was identified by the appearance of a symmetric V-shaped absorption signal centered at $X = 0$. The phase shifter was used to optimize signal symmetry, and the modulation amplitude was reduced to improve precision in determining the exact resonance field.

Measurements were performed at thirteen different frequencies, with the DC current recorded at each resonance condition. To minimize random errors, multiple readings were taken at each frequency setting, and the measurement sequence was repeated to verify reproducibility.

3.3 Documentation of Experimental Setup

Figure 3 shows photographs of the experimental apparatus used for ESR measurements.

(a) Overview of the complete apparatus with all components connected

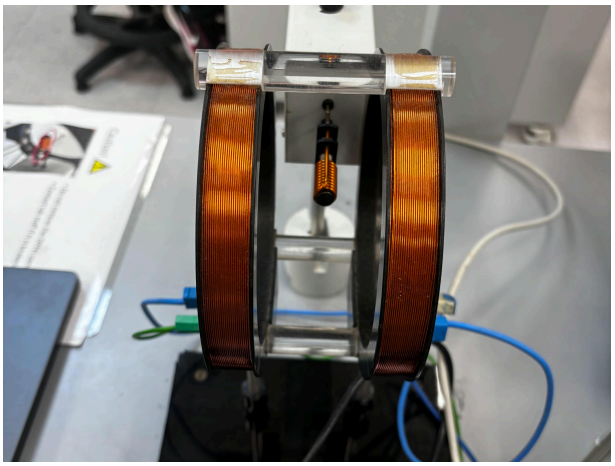

(b) DPPH sample positioned at the center of the Helmholtz coils with RF coil

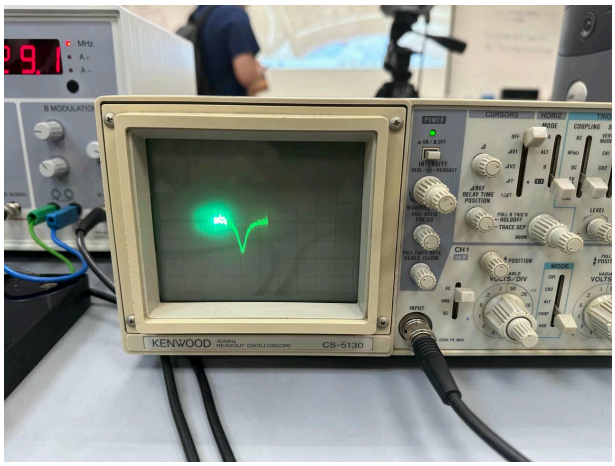

(c) Oscilloscope display showing symmetric V-shaped resonance signal

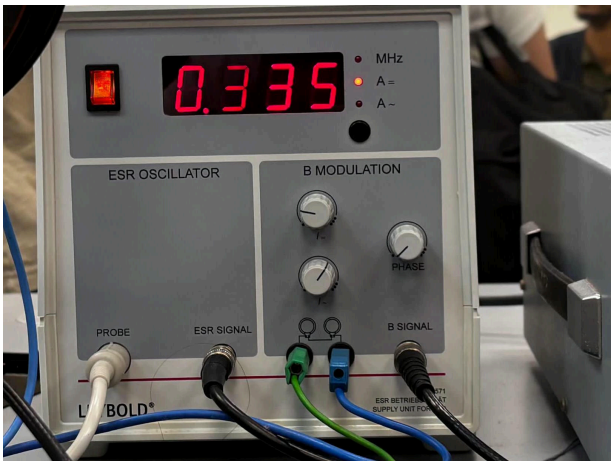

(d) Control unit panel showing frequency and current settings at resonance

Figure 3: Experimental setup for ESR measurements

4 Results and Analysis

4.1 Resonance Mechanism and Signal Detection

To understand the measured data, it is instructive to examine the temporal evolution of the ESR signal. Figure 4 illustrates the relationship between the Zeeman energy level transitions and the resulting detection signal.

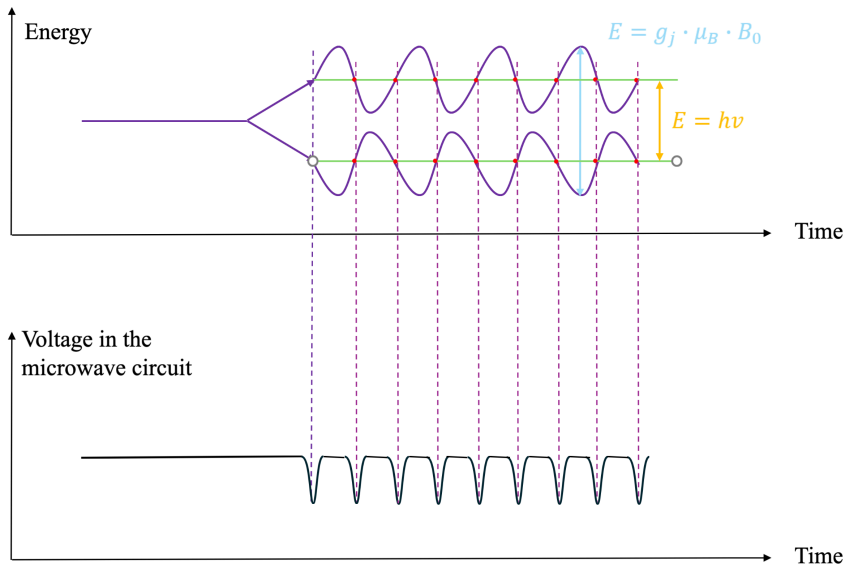

Figure 4: Temporal evolution of ESR signal during measurement.

- **Top panel:** Energy level diagram showing the periodic crossing of the resonance condition as the modulated magnetic field $B = B_0 + B_{\text{mod}} \sin(\omega t)$ varies. The splitting $\Delta E = g_s \mu_B B$ oscillates, causing the system to pass through resonance twice per modulation cycle (red dots indicate absorption events).
- **Bottom panel:** Corresponding voltage response in the RF circuit showing characteristic absorption dips when the resonance condition $h\nu = \Delta E$ is satisfied. The phase relationship between field modulation and signal response is critical for symmetric detection.

This time-domain representation clarifies how the 50 Hz field modulation enables sensitive detection of the resonance condition, producing the characteristic V-shaped signal observed on the oscilloscope when displayed in X-Y mode.

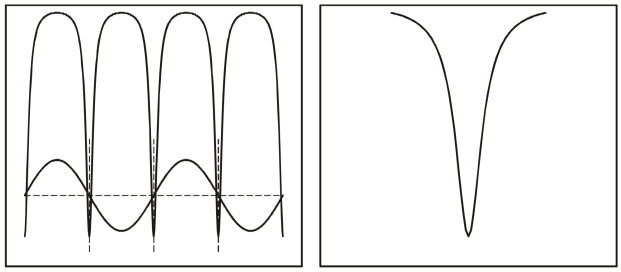

Figure 5: Resonance condition as shown in the oscilloscope.

4.2 Raw Data and Field Calculations

Table 1 presents the measured resonance frequencies and corresponding DC currents, along with the calculated magnetic fields using Equation 4.

Frequency (MHz)	**Current (A)**				**Magnetic Field (mT)**
ν	I_1	I_2	I_3	I_{avg}	B
20.4	0.439	0.443	0.440	0.441	1.88
25.0	0.480	0.483	0.479	0.481	2.05
30.0	0.523	0.520	0.519	0.521	2.221
35.0	0.560	0.566	0.568	0.565	2.408
40.0	0.605	0.598	0.603	0.602	2.566
45.0	0.652	0.644	0.650	0.649	2.767
50.0	0.696	0.700	0.704	0.700	2.984
55.0	0.743	0.747	0.749	0.746	3.180
60.0	0.787	0.784	0.777	0.783	3.338
65.0	0.827	0.824	0.833	0.828	3.530
70.0	0.873	0.870	0.871	0.871	3.713
75.0	0.913	0.926	0.919	0.919	3.917
76.6	0.933	0.942	0.934	0.936	3.990

Table 1: Measured resonance conditions and calculated magnetic fields

4.3 Linear Regression Analysis

According to Equation 3, the relationship between frequency and magnetic field should be linear with slope $k = g_s \frac{\mu_B}{h}$. Figure 6 shows the experimental data with linear fits.

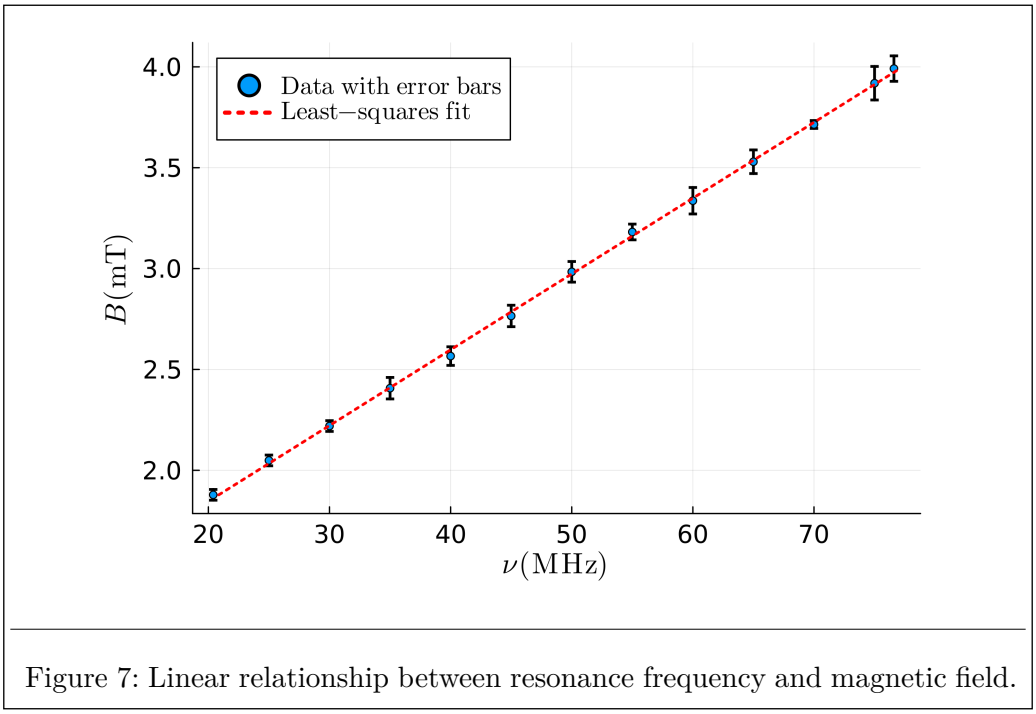

Figure 7: Linear relationship between resonance frequency and magnetic field.

Linear regression of frequency versus magnetic field yielded:

$$\nu = (0.03750 \pm 0.00025)\text{MHz/G} \cdot B + 1.0983 \tag{5}$$

with $R^2 = 0.9995$, indicating excellent linearity.

4.4 g-Factor Determination

From the resonance condition and the measured slope:

$$g_s = \frac{hk}{\mu_B} = \frac{h \cdot \text{slope}}{\mu_B} \tag{6}$$

Converting the slope to SI units: $k = 3.750 \times 10^{13}$ Hz/T

Substituting values:

$$g_s = \frac{(6.626 \times 10^{-34} \text{ J·s})(3.750 \times 10^{13} \text{ Hz/T})}{9.274 \times 10^{-24} \text{ J/T}} = 1.905 \tag{7}$$

4.4.1 Error Analysis

The uncertainty in g_s was determined through error propagation. Starting with the relationship:

$$g_s = \frac{h \cdot \text{slope}}{\mu_B} \tag{8}$$

The relative uncertainty is given by:

$$\frac{\Delta g_s}{g_s} = \sqrt{\left(\frac{\Delta h}{h}\right)^2 + \left(\frac{\Delta(\text{slope})}{\text{slope}}\right)^2 + \left(\frac{\Delta \mu_B}{\mu_B}\right)^2} \tag{9}$$

Since h and μ_B are fundamental constants with negligible uncertainties compared to our experimental precision, the error is dominated by the slope uncertainty:

$$\frac{\Delta g_s}{g_s} \approx \frac{\Delta(\text{slope})}{\text{slope}} = \frac{0.00025}{0.03750} = 0.0067 = 0.67\% \tag{10}$$

However, this represents only the statistical uncertainty from the fit. Additional systematic uncertainties must be considered:

- **Current measurement:** $\Delta I = \pm 0.002$ A (instrumental precision)
$$\frac{\Delta B}{B} = \frac{\Delta I}{I} \approx \frac{0.002}{0.7} = 0.29\% \tag{11}$$
- **Frequency measurement:** $\Delta f = \pm 0.1$ MHz (oscillator stability)
$$\frac{\Delta f}{f} \approx \frac{0.1}{50} = 0.20\% \tag{12}$$
- **Helmholtz coil geometry:** Estimated 1% uncertainty from coil alignment and finite sample size.

Since these instrumental uncertainties (statistical fitting error, current measurement precision, frequency stability, and geometric alignment) are independent sources of error that all contribute to the overall uncertainty in g_s, they are combined in quadrature.

$$\frac{\Delta g_s}{g_s} = \sqrt{(0.0067)^2 + (0.0029)^2 + (0.0020)^2 + (0.010)^2} = 0.013 \tag{13}$$

Therefore:

$$g_s = 1.905 \pm 0.025 \tag{14}$$

5 Discussion

The experimentally determined g-factor of 1.905 ± 0.025 deviates from the theoretical value of 2.0036 by approximately 4.9%. This discrepancy, while outside the calculated uncertainty range, can be attributed to several factors.

Systematic errors likely dominated the uncertainty. The Helmholtz coil equation assumes perfect coil geometry and alignment, but mechanical imperfections and slight misalignment could introduce field inhomogeneities. Additionally, the finite size of the DPPH sample means it experiences a slightly non-uniform field, leading to broadened resonance lines and uncertainty in determining the exact resonance condition.

Instrumental limitations also contributed to measurement uncertainty. The visual determination of resonance on the oscilloscope introduces subjective error, estimated at ± 0.002 A in current readings. The RF frequency stability was specified as ± 0.1 MHz, which becomes more significant at lower frequencies.

Physical considerations specific to DPPH may explain part of the deviation. While DPPH is often approximated as having a free electron g-factor, the actual value is slightly modified by spin-orbit coupling and the molecular environment. Literature values for DPPH typically range from 2.0032 to 2.0038, suggesting our lower value indicates additional systematic effects.

The excellent linearity ($R^2 = 0.9995$) validates the fundamental ESR theory and confirms that systematic rather than random errors dominated. Future improvements could include automated resonance detection, temperature stabilization, and field mapping to characterize inhomogeneities.

6 Conclusion

This experiment successfully demonstrated electron spin resonance in DPPH and determined its g-factor to be 1.905 ± 0.025. The linear relationship between resonance frequency and magnetic field was confirmed with high correlation ($R^2 = 0.9995$), validating the quantum mechanical model of electron spin behavior in magnetic fields. While the measured g-factor showed a 4.9% deviation from the theoretical value of 2.0036, the experiment effectively illustrated the principles of ESR spectroscopy and its application in characterizing paramagnetic materials. The technique's sensitivity to experimental conditions highlights both its power as an analytical tool and the care required for precise measurements.

7 References

1. Beiser, A. *Concepts of Modern Physics*, McGraw-Hill, Singapore, pp. 230-234 (1987).
2. Department of Physics, Universitas Indonesia. *ANP6: Electron Spin Resonance (ESR)* (2020). Available at physics.ui.ac.id.
3. PC2193 ESR Manual (Provided in Canvas)

8 Annex

8.1 Molecular Structure of DPPH

DPPH (2,2-diphenyl-1-picrylhydrazyl) has the molecular formula $C_{18}H_{12}N_5O_6$. The unpaired electron is delocalized over the N-N bond, with significant spin density on the nitrogen atoms. This delocalization contributes to the compound's remarkable stability as a free radical under ambient conditions.

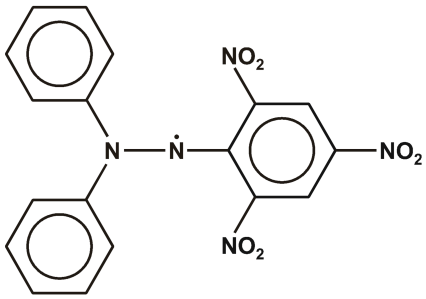

Figure 8: Structure of DPPH

8.2 Anomalous Behavior at Low DC Field

During initial setup procedures, an interesting phenomenon was observed when the DC component of the magnetic field (B_0) was set too low relative to the AC modulation amplitude (B_{mod}). Under these conditions, the modulated magnetic field caused the Zeeman-split energy levels to oscillate with sufficient amplitude that they periodically crossed through the resonance condition $E = h\nu$ twice per modulation cycle.

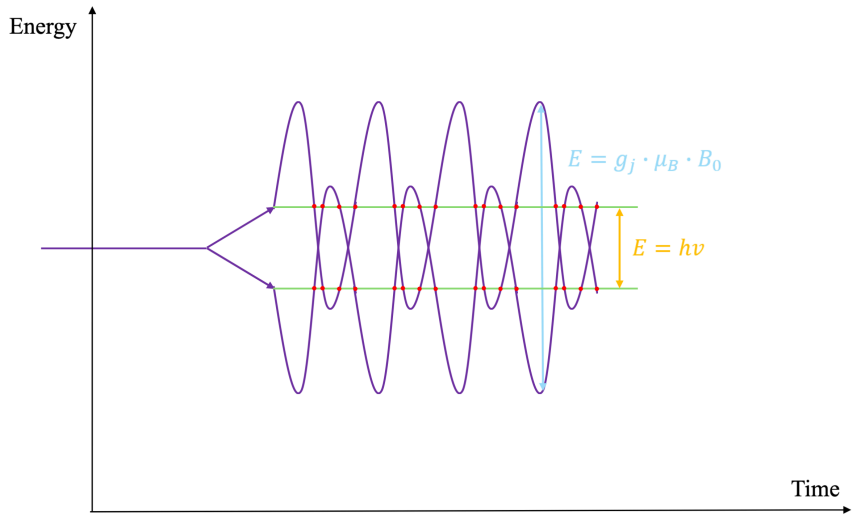

Figure 9: Evolution of energy levels as a function of time with low B_0

This occurs when $B_{\text{mod}} > B_0$, causing the total field $B_{\text{total}} = B_0 + B_{\text{mod}} \sin(\omega t)$ to satisfy the resonance condition $g_j \mu_B B_{\text{total}} = h\nu$ at multiple points during each modulation cycle. The resulting oscilloscope trace showed multiple absorption peaks rather than the single, symmetric resonance signal expected at proper B_0 settings.

This observation highlights the importance of maintaining $B_0 \gg B_{\text{mod}}$ for accurate resonance field determination. When this condition is violated, the system exhibits complex absorption patterns that make precise field measurements impossible. The phenomenon also demonstrates the dynamic nature of the energy level splitting in time-varying magnetic fields and serves as a valuable diagnostic tool for optimizing experimental parameters. For all measurements reported in this work, the DC field was maintained sufficiently high ($B_0 > 5B_{\text{mod}}$) to avoid this complication.

Declaration on the Use of Generative AI

I declare that I **HAVE** used generative AI tools to produce this assignment.

I acknowledge that generative AI was used to produce this assignment in the following manner:

AI Tool Used	**My Prompt and AI Output**	**How the Output Was Used**
ChatGPT	**Prompt:** "How to create a professional LaTeX table with merged cells and proper formatting for scientific data" **Output:** Example code using tabular environment with booktabs package, column specifications, and formatting commands	Used the LaTeX syntax for creating Table 1 with experimental data. Modified column widths and added siunitx formatting for proper unit display. Verified all data values against lab notebook.
ChatGPT	**Prompt:** "Search for theoretical g-factor value of DPPH and typical ESR experimental uncertainties" **Output:** Information about DPPH g-factor (2.0036) and common error sources in ESR measurements including field inhomogeneity and temperature effects	Cross-referenced the theoretical value with course materials and textbook. Used error source information to guide discussion section but calculated actual uncertainties from our experimental data.
Claude 3.5	**Prompt:** "Create professional LaTeX code for inserting experimental setup photos in a 2×2 grid layout" **Output:** LaTeX subfigure environment code with proper formatting and caption structure	Used the provided LaTeX structure for figure placement. Replaced placeholder names with actual photograph filenames and wrote custom captions based on experimental setup.

I confirm that the core experimental work, data collection, and analysis in this report are my own, and the use of generative AI was limited to assistance with LaTeX formatting, technical writing structure, and improving the clarity of scientific explanations.